Tight-binding calculation of radiation loss in photonic crystal CROW

Jing Ma,[1,3] Luis Javier Martínez,[1,3] Shanhui Fan,[2] and Michelle L. Povinelli[1,*]

[1]*Ming Hsieh Department of Electrical Engineering, University of Southern California, Powell Hall of Engineering, 3737 Watt Way, Los Angeles, Californai 90089-0271, USA*

[2]*Ginzton Laboratory and the Department of Electrical Engineering, Stanford University, Stanford, California 94305, USA*

[3]Both authors contributed equally to this work

[*]*povinell@usc.edu*

Abstract: The tight binding approximation (TBA) is used to relate the intrinsic, radiation loss of a coupled resonator optical waveguide (CROW) to that of a single constituent resonator within a light cone picture. We verify the validity of the TBA via direct, full-field simulation of CROWs based on the L2 photonic crystal cavity. The TBA predicts that the quality factor of the CROW increases with that of the isolated cavity. Moreover, our results provide a method to design CROWs with low intrinsic loss across the entire waveguide band.

OCIS codes: (160.5298) Photonic crystals; (130.5296) Photonic crystal waveguides; (230.4555) Coupled resonators.

References and links

1. A. Yariv, Y. Xu, R. K. Lee, and A. Scherer, "Coupled-resonator optical waveguide: a proposal and analysis," Opt. Lett. **24**(11), 711–713 (1999).
2. R. M. De La Rue, "Optical delays: slower for longer," Nat. Photonics **2**(12), 715–716 (2008).
3. N. Stefanou and A. Modinos, "Impurity bands in photonic insulators," Phys. Rev. B **57**(19), 12127–12133 (1998).
4. M. F. Yanik and S. Fan, "Stopping light all optically," Phys. Rev. Lett. **92**(8), 083901 (2004).
5. S. Sandhu, M. L. Povinelli, M. F. Yanik, and S. Fan, "Dynamically tuned coupled-resonator delay lines can be nearly dispersion free," Opt. Lett. **31**(13), 1985–1987 (2006).
6. J. K. Poon, L. Zhu, G. A. DeRose, and A. Yariv, "Transmission and group delay of microring coupled-resonator optical waveguides," Opt. Lett. **31**(4), 456–458 (2006).
7. F. Morichetti, A. Melloni, A. Breda, A. Canciamilla, C. Ferrari, and M. Martinelli, "A reconfigurable architecture for continuously variable optical slow-wave delay lines," Opt. Express **15**(25), 17273–17282 (2007).
8. F. Xia, L. Sekaric, and Y. Vlasov, "Ultracompact optical buffers on a silicon chip," Nat. Photonics **1**(1), 65–71 (2007).
9. S. Olivier, C. Smith, M. Rattier, H. Benisty, C. Weisbuch, T. Krauss, R. Houdré, and U. Oesterlé, "Miniband transmission in a photonic crystal coupled-resonator optical waveguide," Opt. Lett. **26**(13), 1019–1021 (2001).
10. E. Ozbay, M. Bayindir, I. Bulu, and E. Cubukcu, "Investigation of localized coupled-cavity modes in two-dimensional photonic bandgap structures," IEEE J. Quantum Electron. **38**(7), 837–843 (2002).
11. T. J. Karle, D. H. Brown, R. Wilson, M. Steer, and T. E. Krauss, "Planar photonic crystal coupled cavity waveguides," IEEE J. Sel. Top. Quantum Electron. **8**(4), 909–918 (2002).
12. P. Sanchis, J. Marti, W. Bogaerts, P. Dumon, D. Van Thourhout, and R. Baets, "Experimental results on adiabatic coupling into SOI photonic crystal coupled-cavity waveguides," IEEE Photon. Technol. Lett. **17**(6), 1199–1201 (2005).
13. D. O'Brien, M. D. Settle, T. Karle, A. Michaeli, M. Salib, and T. F. Krauss, "Coupled photonic crystal heterostructure nanocavities," Opt. Express **15**(3), 1228–1233 (2007).
14. J. Jágerská, N. Le Thomas, V. Zabelin, R. Houdré, W. Bogaerts, P. Dumon, and R. Baets, "Experimental observation of slow mode dispersion in photonic crystal coupled-cavity waveguides," Opt. Lett. **34**(3), 359–361 (2009).
15. J. Jágerská, H. Zhang, N. Le Thomas, and R. Houdré, "Radiation loss of photonic crystal coupled-cavity waveguides," Appl. Phys. Lett. **95**(11), 111105 (2009).
16. N. Matsuda, T. Kato, K.-i. Harada, H. Takesue, E. Kuramochi, H. Taniyama, and M. Notomi, "Slow light enhanced optical nonlinearity in a silicon photonic crystal coupled-resonator optical waveguide," Opt. Express **19**(21), 19861–19874 (2011).
17. H.-C. Liu and A. Yariv, "Designing coupled-resonator optical waveguides based on high-Q tapered grating-defect resonators," Opt. Express **20**(8), 9249–9263 (2012).

#179666 - $15.00 USD Received 12 Nov 2012; revised 21 Dec 2012; accepted 10 Jan 2013; published 25 Jan 2013

18. Y. Kawaguchi, K. Saitoh, and M. Koshiba, "Analysis of leakage losses in one-dimensional photonic crystal coupled resonator optical waveguide using 3-D finite element method," J. Lightwave Technol. **28**(20), 2977–2983 (2010).
19. A. Martínez, J. García, P. Sanchis, F. Cuesta-Soto, J. Blasco, and J. Martí, "Intrinsic losses of coupled-cavity waveguides in planar-photonic crystals," Opt. Lett. **32**(6), 635–637 (2007).
20. M. L. Povinelli and S. Fan, "Radiation loss of coupled-resonator waveguides in photonic-crystal slabs," Appl. Phys. Lett. **89**(19), 191114 (2006).
21. D. P. Fussell and M. M. Dignam, "Engineering the quality factors of coupled-cavity modes in photonic crystal slabs," Appl. Phys. Lett. **90**(18), 183121 (2007).
22. T. Tanabe, M. Notomi, E. Kuramochi, A. Shinya, and H. Taniyama, "Trapping and delaying photons for one nanosecond in an ultrasmall high-Q photonic-crystal nanocavity," Nat. Photonics **1**(1), 49–52 (2007).
23. J. Vuckovic, M. Loncar, H. Mabuchi, and A. Scherer, "Optimization of the Q factor in photonic crystal microcavities," IEEE J. Quantum Electron. **38**(7), 850–856 (2002).
24. L. C. Andreani and D. Gerace, "Photonic-crystal slabs with a triangular lattice of triangular holes investigated using a guided-mode expansion method," Phys. Rev. B **73**(23), 235114 (2006).
25. Y. Xu, R. K. Lee, and A. Yariv, "Propagation and second-harmonic generation of electromagnetic waves in a coupled-resonator optical waveguide," J. Opt. Soc. Am. B **17**(3), 387–400 (2000).
26. A. Taflove, *Computational Electrodynamics: the Finite-Difference Time-Domain Method* (Artech House, 1995).
27. A. R. A. Chalcraft, S. Lam, D. O'Brien, T. F. Krauss, M. Sahin, D. Szymanski, D. Sanvitto, R. Oulton, M. S. Skolnick, A. M. Fox, D. M. Whittaker, H. Y. Liu, and M. Hopkinson, "Mode structure of the L3 photonic crystal cavity," Appl. Phys. Lett. **90**(24), 241117 (2007).
28. C. A. Mejia, A. Dutt, and M. L. Povinelli, "Light-assisted templated self assembly using photonic crystal slabs," Opt. Express **19**(12), 11422–11428 (2011).
29. J. Ma, L. J. Martínez, and M. L. Povinelli, "Optical trapping via guided resonance modes in a Slot-Suzuki-phase photonic crystal lattice," Opt. Express **20**(6), 6816–6824 (2012).

1. Introduction

Coupled resonator optical waveguides (CROWs) [1], waveguides in which light propagates by "hopping" between localized resonator modes, have been widely studied for application to on-chip optical delays [2]. CROWs provide both slow group velocity and low dispersion [3], essential features for distortion-free signal delay. In dynamically-tuned CROWs, light pulses may be stopped, stored, and released on demand [4,5]. CROWs based on various resonator types have been investigated, including microring resonators [6–8] and photonic-crystal microcavities [9–15]. We focus here on photonic-crystal microcavity CROWs, which provide both compact resonator size and high spatial confinement; the latter is useful, for example, for achieving nonlinear effects at low power levels [16].

Minimization of propagation loss is an important aspect of CROW design. Various approaches have been used to design low-loss CROWs, including coupled-mode theory [17] and the finite-element method [18]. CROWs formed by microcavities in photonic-crystal slabs are intrinsically lossy, because the CROW mode lies above the light line of air, the mode leaks light vertically as it propagates [19]. Moreover, if the loss is uneven across the CROW band for different wavevectors, the effective transmission bandwidth is reduced, and the transmitted signal is distorted. The intrinsic loss provides a lower bound on the total loss, which may also include contributions due to fabrication imperfections and scattering.

Previous theoretical work has shown that intrinsic CROW loss can depend strongly on frequency and be up to an order of magnitude larger or smaller than that of an individual resonator [20,21]. At the same time, experiments have demonstrated particular CROW designs with low loss comparable to that of an individual resonator [22]. Given these considerations, it is important to understand theoretically how the CROW and resonator losses are related, as well as how to achieve low, flat loss across the entire CROW bandwidth. In this paper, we use a model based on the tight-binding approximation (TBA) to answer these questions.

TBA approaches are advantageous, as they allow the calculation of the frequency-dependent loss of a CROW from a single, full-field simulation of an individual cavity. Previously, Fussell and Dignam have used a TBA model based on the complex dispersion relation of the CROW to calculate losses [21]. Another approach is to use the TBA to relate the electromagnetic fields of the CROW to those of the isolated cavity [15]. In this case, the spatial power spectrum of the CROW fields may be obtained from that of the isolated cavity by taking discrete samples in Fourier space, as experimentally demonstrated in [15].

#179666 - $15.00 USD Received 12 Nov 2012; revised 21 Dec 2012; accepted 10 Jan 2013; published 25 Jan 2013

Reference [15] has suggested that the losses may then be calculated from the power spectrum using a light-cone picture [23]. In this paper, we explicitly demonstrate the validity of this approach by comparing the predictions of the TBA light-cone model with direct calculations. We then show that within a particular family of photonic-crystal cavities, a decrease in cavity loss also results in a decrease in CROW loss. While the CROW loss generally varies across the CROW band, we show that the TBA predicts particular cavity separations for which the loss is flat.

2. Theoretical formulation of CROW quality factor in the tight-binding approximation

For concreteness, we first consider the CROW structure shown in Fig. 1(a). The photonic crystal slab is a triangular lattice of air holes with lattice constant a and hole radius $r = 0.29a$ in a suspended, dielectric slab with height $0.6a$ and refractive index $n = 3.45$ (silicon at a wavelength of 1.55μm). The CROW waveguide consists of periodically spaced defects. Each defect is a micro-cavity with two adjacent missing holes, known as an L2 cavity. The center-to-center spacing of adjacent defects is $5a$. The separation width S, the width of the region between defects that does not contain missing holes, is $3a$. We denote the CROW as LmSn, with m being the number of missing holes of the constituent cavity and n the number of separation holes. We calculate the band structure by the guided-mode expansion method [24]. Figure 1(b) shows the dispersion relations for L2S2, L2S3, and L2S4 CROWs, respectively. The band of each CROW mode displays a cosinusoidal shape [1,3], with the center frequency close to the fundamental mode of the isolated L2 cavity, $0.26992(2\pi c/a)$. The bandwidth of a CROW mode is proportional to the coupling strength between adjacent defects. Figure 1(b) shows that the coupling strength decreases as the separation is increased.

For all three CROWs, the CROW band lies above the light line of air and is thus intrinsically lossy. The light line of air is given by $\omega = ck$, where k is the in-plane CROW wavevector. At the edge of the Brillouin zone, $k = k_{Bz} \equiv \pi / D$ and the light-line frequency $\omega = 0.125(2\pi c/a)$, $0.1(2\pi c/a)$, or $0.083(2\pi c/a)$ for $D = 4a$, $D = 5a$ or $D = 6a$, respectively. In all three cases, the upper edge of the light line lies well below the frequency range shown in Fig. 1(b).

We define a waveguide quality factor $Q(k)$ to describe the leakage of the CROW mode:

$$Q(k) = \omega(k)\tau_{1/e} \tag{1}$$

where $\omega(k)$ is the dispersion relation of the CROW mode, and $\tau_{1/e}$ is the time in which the power in the waveguide mode decays by $1/e$. $Q(k)$ can be converted to a $1/e$ power-decay length in the waveguide as $L_{1/e}(k) = v_g(k)Q(k)/\omega(k)$, where $v_g(k)$ is the group velocity.

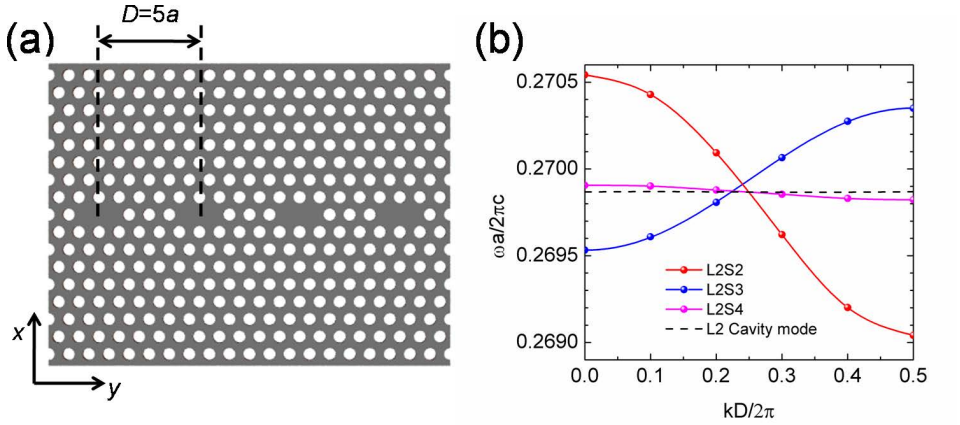

Fig. 1. (a) Schematic diagram of CROW structure L2S3. (b) Dispersion curve of CROW mode in L2S2 (red), L2S3 (blue) and L2S4 (magenta). Dashed line shows the fundamental mode of the isolated L2 cavity.

#179666 - $15.00 USD Received 12 Nov 2012; revised 21 Dec 2012; accepted 10 Jan 2013; published 25 Jan 2013

Alternately, the loss in dB/length is equal to $-4.34\text{dB}/L_{1/e}$. While the loss per unit length diverges at $k = 0$ and $0.5(2\pi/\text{D})$ where $v_g = 0$, $Q(k)$ is well defined over the entire Brillouin zone.

2.1. Light line picture

For isolated microcavities, it has been shown [23] that the cavity Q can be related to the Fourier transform of the electromagnetic fields above the surface of the slab. A similar relation is true for the waveguide quality factor $Q(k)$.

We can write

$$Q(k) = \omega(k)\frac{\langle U(k)\rangle}{\langle P(k)\rangle} \tag{2}$$

where $\langle U(k)\rangle$ is the time-averaged electromagnetic field energy:

$$\langle U(k)\rangle = \frac{1}{2}\iiint_V dV\left(\varepsilon_{CROW}(x,y,z)\left|\vec{E}_k(x,y,z)\right|^2 + \mu_o\left|\vec{H}_k(x,y,z)\right|^2\right), \tag{3}$$

where $\varepsilon_{CROW}(x,y,z)$ is the dielectric constant of the CROW, and $\vec{E}_k(x,y,z)$ and $\vec{H}_k(x,y,z)$ are the electric and magnetic fields of the CROW mode at wave vector k. $\langle P(k)\rangle$ is the time-averaged emitted power,

$$\langle P(k)\rangle = \oiint_S d\vec{S}\cdot\frac{1}{2}\text{Re}\left(\vec{E}_k(x,y,z)\times\vec{H}_k^*(x,y,z)\right), \tag{4}$$

where the integral is over a closed surface that encloses the photonic crystal slab. For an infinitely long CROW, both $\langle U(k)\rangle$ and $\langle P(k)\rangle$ are infinite; however, the ratio $\langle U(k)\rangle/\langle P(k)\rangle$ is finite and equal to the value of the ratio for a single unit cell.

$\langle P(k)\rangle$ can be rewritten in terms of the two-dimensional (2D) spatial power spectra of the free-space fields, on any surface above the structure [23]:

$$\begin{aligned}\langle P(k)\rangle = \frac{1}{2}\sqrt{\frac{\mu_o}{\varepsilon_o}}\iint_{q_\parallel\le\omega(k)/c}\frac{dq_x}{2\pi}\frac{dq_y}{2\pi}\Bigg\{&\frac{\varepsilon_o}{\mu_o}\left(\left|\tilde{E}_{k,x}(q_x,q_y)\right|^2+\left|\tilde{E}_{k,y}(q_x,q_y)\right|^2\right)\\&+\left(\left|\tilde{H}_{k,x}(q_x,q_y)\right|^2+\left|\tilde{H}_{k,y}(q_x,q_y)\right|^2\right),\end{aligned} \tag{5}$$

where $q_\parallel = \left(q_x^{\,2}+q_y^{\,2}\right)^{1/2}$ and $\tilde{E}_{k,i}(q_x,q_y)$ and $\tilde{H}_{k,i}(q_x,q_y)$ are the 2D Fourier transforms of the ith component of $\vec{E}_k(x,y,z)$ and $\vec{H}_k(x,y,z)$, and $(i\in x,y)$:

$$\begin{aligned}\tilde{E}_{k,i}(q_x,q_y) &= \iint dxdy\,E_{k,i}(x,y)e^{-i\left(q_x x+q_y y\right)}\\ \tilde{H}_{k,i}(q_x,q_y) &= \iint dxdy\,H_{k,i}(x,y)e^{-i\left(q_x x+q_y y\right)}\end{aligned} \tag{6}$$

The Fourier-space integral includes all $q_\parallel$ within the light cone $\left(q_\parallel\le\omega/c\right)$. Only these so-called "leaky components" contribute to radiation loss. We will refer to the quantities $\left|\tilde{E}_{k,x}(q_x,q_y)\right|^2$, $\left|\tilde{E}_{k,y}(q_x,q_y)\right|^2$, $\left|\tilde{H}_{k,x}(q_x,q_y)\right|^2$, and $\left|\tilde{H}_{k,y}(q_x,q_y)\right|^2$ appearing in Eq. (5) as the E_x, E_y, H_x, and H_y power spectra, respectively.

#179666 - $15.00 USD Received 12 Nov 2012; revised 21 Dec 2012; accepted 10 Jan 2013; published 25 Jan 2013

Due to the periodicity of the CROW waveguide in the *x*-direction, Fourier transforms of the field components are only nonzero for discrete values of q_x. Using Bloch's theorem, the CROW mode can be written as $\vec{E}_k(x,y,z) = e^{ikx}\vec{U}_k(x,y,z)$, where $\vec{U}_k(x+D,y,z) = \vec{U}_k(x,y,z)$. An analogous statement is true for $\vec{H}_k(x,y,z)$. It follows that the Fourier transforms $\tilde{E}_{k,i}(q_x,q_y) = \tilde{H}_{k,i}(q_x,q_y) = 0$ except when $q_x = k + 2\pi n / D$. The Fourier transforms are nonzero over a continuous range of q_y values.

2.2. Tight-binding approximation

The tight-binding approximation can be used to write the CROW quality factor in terms of the fields of the isolated cavity.

First, we write the CROW fields in terms of the isolated cavity fields $\vec{E}_\Omega(x,y,z)$ and $\vec{H}_\Omega(x,y,z)$:

$$\begin{aligned}\vec{E}_k(x,y) &= E_0 \sum_{n=-\infty}^{\infty} e^{inkD}\vec{E}_\Omega(x-nD,y,z)\\ \vec{H}_k(x,y) &= H_0 \sum_{n=-\infty}^{\infty} e^{inkD}\vec{H}_\Omega(x-nD,y,z)\end{aligned} \tag{7}$$

where E_0 and H_0 are normalization constants [1]. Taking into account that

$$\sum_{n=-\infty}^{\infty} e^{-inx} = 2\pi\sum_{l=-\infty}^{\infty}\delta(x-2\pi l) \tag{8}$$

it follows that

$$\begin{aligned}\left|\tilde{E}_{k,i}(q_x,q_y)\right|^2 &= \left|E_0\right|^2\left(\frac{2\pi}{D}\right)\sum_{m=-\infty}^{\infty}\sum_{n=-\infty}^{\infty}\delta\left(q_x - k - \frac{2\pi n}{D}\right)\left|\tilde{E}_{\Omega,i}(q_x,q_y)\right|^2\\ \left|\tilde{H}_{k,i}(q_x,q_y)\right|^2 &= \left|H_0\right|^2\left(\frac{2\pi}{D}\right)\sum_{m=-\infty}^{\infty}\sum_{n=-\infty}^{\infty}\delta\left(q_x - k - \frac{2\pi n}{D}\right)\left|\tilde{H}_{\Omega,i}(q_x,q_y)\right|^2\end{aligned} \tag{9}$$

where the sum over *m* can be interpreted as a sum over unit cells. This relation is schematically depicted in Fig. 2(a). The tight-binding approximation predicts that for fixed q_y, the power spectrum of each field component of the CROW mode is given by a set of delta-

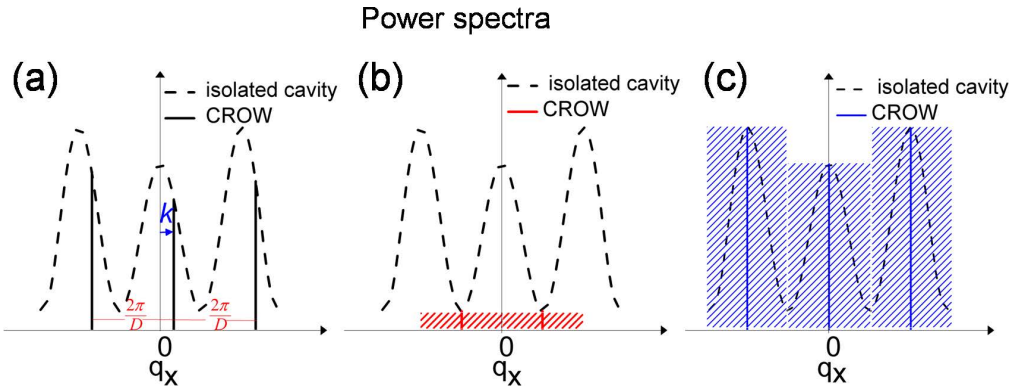

Fig. 2. (a) Schematic picture of tight-binding prediction for the power spectrum of a CROW mode. (b) CROW power spectrum giving a large value of $Q(k)$ compared to the isolated cavity. (c) CROW Power spectrum giving a small value of $Q(k)$ compared to the isolated cavity.

#179666 - $15.00 USD Received 12 Nov 2012; revised 21 Dec 2012; accepted 10 Jan 2013; published 25 Jan 2013

function spikes weighted by the power spectrum of the isolated cavity. The spikes are shifted by k, and the separation between neighboring spikes is $2\pi / D$.

Within the tight-binding approximation, $\langle P(k) \rangle$ can be found by substituting Eq. (9) into Eq. (5). $\langle U(k) \rangle$ can be found by substituting Eq. (7) into Eq. (3):

$$\langle U(k) \rangle = \frac{1}{2} \iiint_V dV \left\{ \varepsilon_{CROW}(x,y,z) E_0^2 \sum_{n=-\infty}^{\infty} \sum_{m=-\infty}^{\infty} e^{i(n-m)kD} \vec{E}_\Omega^*(x-nD,y,z) \vec{E}_\Omega(x-mD,y,z) \right.$$
$$\left. + H_0^2 \sum_{n=-\infty}^{\infty} \sum_{m=-\infty}^{\infty} e^{i(n-m)kD} \vec{H}_\Omega^*(x-nD,y,z) \vec{H}_\Omega(x-mD,y,z) \right\} \tag{10}$$

The $m = n$ terms will dominate, leading to the approximation that

$$\langle U \rangle \approx \frac{1}{2} \sum_{m=-\infty}^{\infty} \iiint_V dV \left\{ \varepsilon_{CROW}(x,y,z) E_0^2 \left| \vec{E}_\Omega(x,y,z) \right|^2 + \mu_o H_0^2 \left| \vec{H}_\Omega(x,y,z) \right|^2 \right\}, \tag{11}$$

independent of k. For weak coupling between defects, we substitute ε_Ω, the dielectric function of the isolated cavity, for ε_{CROW}, and

$$\begin{aligned} \langle U \rangle &\approx \frac{1}{2} \sum_{m=-\infty}^{\infty} \iiint_V dV \left\{ \varepsilon_\Omega(x,y,z) E_0^2 \left| \vec{E}_\Omega(x,y,z) \right|^2 + \mu_0 H_0^2 \left| \vec{H}_\Omega(x,y,z) \right|^2 \right\} \\ &\approx \sum_{m=-\infty}^{\infty} \langle U_\Omega \rangle \end{aligned} \tag{12}$$

where U_Ω is the field energy of the isolated cavity.

Using the expressions for $\langle P(k) \rangle$ and $\langle U(k) \rangle$, the final result is that

$$Q(k) \approx \omega_o \langle U_\Omega \rangle \left[\frac{1}{2} \sqrt{\frac{\mu_o}{\varepsilon_o}} \left(\frac{2\pi}{D} \right) \iint_{q_\parallel \le \omega/c} \frac{dq_x}{2\pi} \frac{dq_y}{2\pi} \sum_{n=-\infty}^{\infty} \delta\left(q_x - k - \frac{2\pi n}{D} \right) \times \right.$$
$$\left. \left\{ \frac{\varepsilon_o}{\mu_o} \left(\left| \tilde{E}_{\Omega,x}(q_x,q_y) \right|^2 + \left| \tilde{E}_{\Omega,y}(q_x,q_y) \right|^2 \right) + \left| \tilde{H}_{\Omega,x}(q_x,q_y) \right|^2 + \left| \tilde{H}_{\Omega,y}(q_x,q_y) \right|^2 \right\} \right]^{-1} \tag{13}$$

Here, we have assumed that the variation in ω across the CROW band, $\Delta\omega$, is small compared to the isolated cavity frequency ω_0. In this case, $\omega(k)$ can be approximated by ω_0 in Eq. (13). For the numerical examples presented below, $\Delta\omega/\omega_0$ is on the order of 10^{-3}.

Equation (13) implies that within the tight-binding approximation, increasing Q_0 of the isolated cavity will tend to increase the $Q(k)$ of the corresponding waveguide. This is because an increase in Q_0 corresponds to a decrease in the power spectra values of the isolated cavity within the light cone. However, due to the discrete nature of the sum, $Q(k)$ can have a strong dependence on the wave vector. This is illustrated schematically in Figs. 2(b) and 2(c). For a particular value of k, it may happen that the spikes in the CROW power spectrum line up with minima (Fig. 2(b)) or maxima (Fig. 2(c)) of the isolated cavity power spectrum. The Q_0 of the isolated cavity is inversely proportional to the area under the dashed line, while $Q(k)$ of the CROW mode is inversely proportional to the red or blue dashed areas shown. It is apparent that the dashed area can either be smaller (Fig. 2(b)) or larger (Fig. 2(c)) than the area under the curve. As a result, $Q(k)$ can be either larger or smaller than Q_0.

In general, the validity of the TBA improves as the separation between cavities increases. For decreasing separation, as the fields of neighboring cavities interact more strongly, it becomes less accurate to write the CROW fields in terms of the isolated cavity mode (Eq. (7). We note that in the numerical examples below, we consider cavities in which the modes are

#179666 - $15.00 USD Received 12 Nov 2012; revised 21 Dec 2012; accepted 10 Jan 2013; published 25 Jan 2013

well isolated and the spacing between modes is large compared to the width of the CROW band. In some CROW's, the simple model of a well isolated mode is not sufficient, and coupling with other modes of the isolated cavity must be considered. In this case, Eq. (7) would be modified to include a sum over multiple cavity modes. The expansion coefficients in the sum can be found as in Ref [25], and Eqs. (10) and 13 would be similarly modified. In cases where nearest neighbor or next-nearest neighbor coupling are significant, the $m-n\neq 0$ terms should be included in the calculation of $\langle U(k)\rangle$ (Eq. (10).

3. Numerical validation of the tight binding approximation

To test the TBA model of the CROW quality factor, we perform three-dimensional finite-difference time-domain (FDTD) simulations [26] of $Q(k)$ for CROW structures and compare the results with the TBA prediction of Eq. (13). We start with CROW structures based on the L2 cavity, such as the one shown above in Fig. 1(a).

For the isolated cavity simulation, a computational cell of $35a\times 10\sqrt{3}a\times 4a$ was used. Perfectly-matched layer (PML) boundaries were used in all directions, and the grid resolution was 20 grid points per a. In Fig. 3(a), we plot E_y for the fundamental mode of the L2 cavity on a plane $0.2a$ above the slab surface. The mode is antisymmetric with respect to both the x-z plane and y-z planes. Figure 3(b) shows the E_y power spectrum, $\left|\tilde{E}_{\Omega,y}(q_x,q_y)\right|^2$ for the isolated

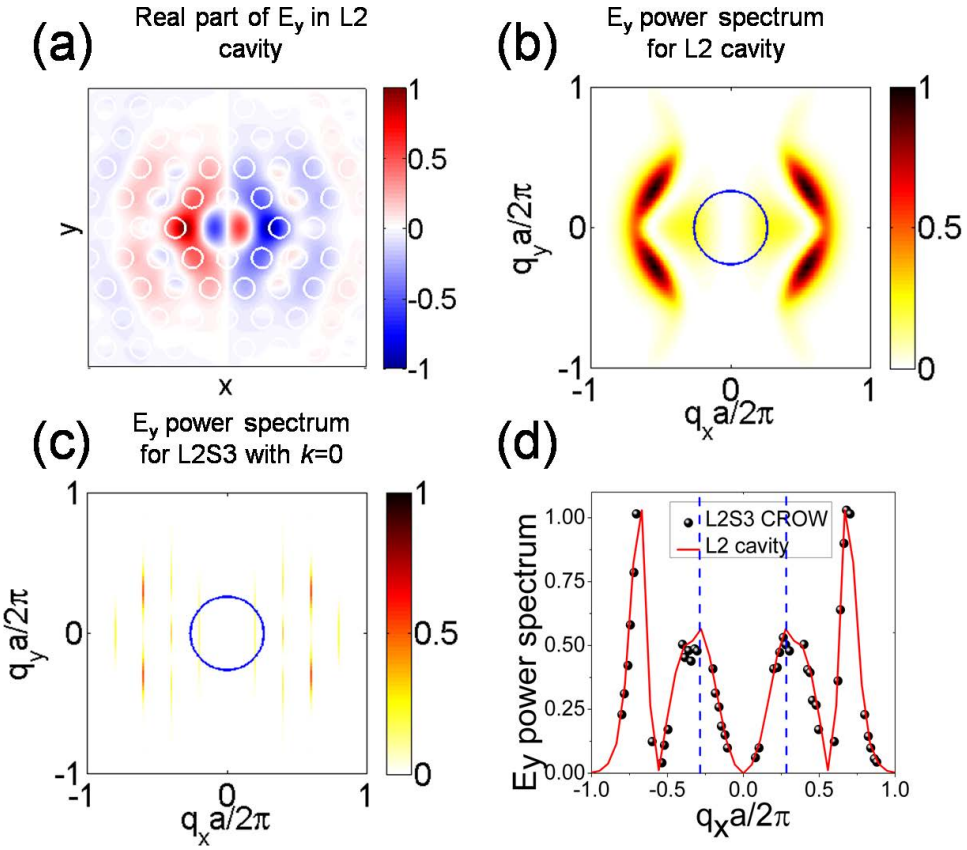

Fig. 3. (a) Mode distribution of the real part of E_y on the x-y plane $0.2a$ above the surface of the isolated L2 cavity. (b) Power spectrum of L2 cavity. The blue circle is the light cone. (c) Power spectrum of CROW mode in L2S3 structure with $k = 0$. (d) Visual test of tight-binding approximation via comparison of CROW power spectra to that of isolated L2 cavity. The blue dashed lines indicate light lines.

#179666 - $15.00 USD Received 12 Nov 2012; revised 21 Dec 2012; accepted 10 Jan 2013; published 25 Jan 2013

cavity. We note that the power spectrum is zero along $q_x = 0$, due to the fact that $E_{\Omega,y}$ is odd with respect to $x = 0$. In Figs. 3(a) and 3(b), the field magnitude and power spectrum are each normalized to their maximum values.

We next calculate the full CROW fields and corresponding power spectrum. We use the FDTD method to simulate a single unit cell of the L2S3 CROW. The boundary conditions are fixed to be Bloch-periodic in the *x*-direction with fixed wave vector *k*. In the *y*-direction, the length of the computational cell is chosen to be large enough ($10\sqrt{3}a$) for $Q(k)$ to be independent of length. Perfectly-matched layer boundaries are applied in the *y* and *z* directions. The grid resolution was 20 points per *a*. We divide the calculated field components by e^{ikx} to obtain the periodic field envelopes. We then Fourier transform the envelopes and shift them by *k* in the q_x-direction, a procedure that can easily be shown to yield $\left|\tilde{E}_{k,i}(q_x, q_y)\right|^2$ and $\left|\tilde{H}_{k,i}(q_x, q_y)\right|^2$. In Fig. 3(c), we plot the E_y power spectrum of the L2S3 CROW mode for $k = 0$. The CROW power spectrum is only nonzero at discrete values of q_x separated by a distance $\Delta q_x = (1/5)(2\pi/a) = 0.2(2\pi/a)$. In this case, only three values of q_x fall within the light cone, $q_x = 0$ and $q_x = \pm 0.2(2\pi/a)$. The power spectrum is zero for $q_x = 0$, since E_y is odd with respect to $x = 0$.

Within the TBA, the CROW power spectrum can be found by using the Dirac delta function to sample the power spectrum of the isolated cavity mode (Eq. (9)). To test this approximation quantitatively, we plot the values of the L2 isolated cavity power spectrum (red curve) and the L2S3 CROW power spectra (black dots) along $q_y = 0$ in Fig. 3(d). Multiple values of *k* are shown on the same plot, and the blue dashed lines indicate the position of the light lines. The overall agreement is quite good.

As a further check of the TBA model, we quantitatively compare the results for $Q(k)$ to those obtained by direct simulation of the full CROW structure. Figure 4 shows results for CROW waveguides with varying separation between cavities: Figs. 4(a)–4(c) correspond to L2S2, L2S3, and L2S4 CROWs, respectively. Q_o for the isolated cavity is shown by the red lines and has a value of 1440.

The results labeled "FDTD" and "FDTD-LC" represent two different, direct methods for calculating $Q(k)$ from the full CROW structure. In both cases, a Bloch periodic unit cell with fixed *k* was used, as described above. A narrowband, pulsed source was used to excite the mode of interest. In the first case ("FDTD," black lines) $Q(k)$ was calculated from the field decay time after source turn-off. In the second case ("FDTD-LC", magenta lines), $Q(k)$ was instead calculated from an integral over the CROW fields via the light-cone approach (Eqs. (2-5). The agreement between the two direct methods is good, indicating the validity of the light-cone formulation for CROW modes. For high-Q modes, one might expect the "FDTD" method to be more accurate than the "FDTD-LC" method, which depends on an integral over

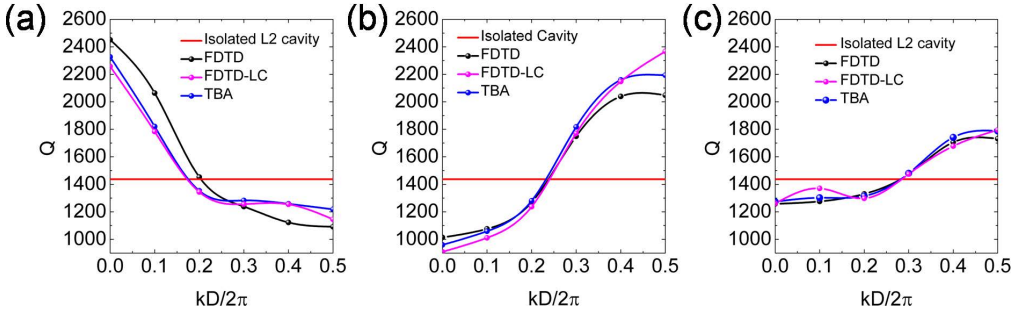

Fig. 4. $Q(k)$ for L2 CROWs with varying cavity separations: (a) L2S2, (b) L2S3, and (c) L2S4. Dots represent calculated values. Lines represent guides for the eye.

#179666 - $15.00 USD Received 12 Nov 2012; revised 21 Dec 2012; accepted 10 Jan 2013; published 25 Jan 2013

small field components and may therefore be more susceptible to numerical error than the extraction of a decay time.

The results labeled "TBA" are obtained by using the tight-binding approximation to calculate $Q(k)$ from the isolated cavity mode, via Eq. (13) (blue lines). The TBA is shown to predict the $Q(k)$ well. The maximum difference between the TBA method and the FDTD method is 12% for L2S2, 7% for L2S3, and 3% for L2S4. As expected, the accuracy of the TBA improves with increasing cavity separation. Importantly, using the TBA allows the prediction of the entire $Q(k)$ curve for all three CROWs from only a single calculation of the isolated cavity mode.

From Fig. 4, we notice that the k-dependence of the CROW quality factor, $Q(k)$, is not universal. Q may increase or decrease with k, depending on cavity separation. For all three cases shown (L2S2, L2S3, and L2S4), the minimum and maximum values of $Q(k)$ occur at either $k = 0$ or $k = k_{Bz} = 0.5(2\pi / D)$. Depending on k, the CROW mode can have either a higher or lower quality factor than the isolated cavity. In the middle of the Brillouin zone, the quality factors are similar. At $k = 0.25(2\pi / D)$, the difference between $Q(k)$ of the CROW and Q_o of the isolated cavity is below 10% for all three cavity separations shown.

Interestingly, while the L2 cavity mode cannot emit light vertically due to symmetry considerations [27], the CROW can. For the isolated cavity, symmetry prohibits coupling to a plane wave propagating in the z-direction. However, leakage occurs in off-normal directions, yielding a finite quality factor. For the CROW mode at $Q(k = 0)$, symmetry again prohibits coupling to a z-propagating plane wave. However, translational symmetry requires that any leakage be in the z-direction. The finite value of $Q(k = 0)$ indicates that vertical leakage does occur; in this case, it arises from interference between off-normal plane waves radiated from the individual cavities.

4. Factors influencing the CROW quality factor

The results above verify that the TBA model is a good predictor of $Q(k)$ in CROWs based on the L2 cavity. Using the TBA, we can gain insight into how the CROW quality factor depends on wave vector, cavity separation, and the quality factor of the isolated cavity.

In Fig. 5, we plot $Q(k)$ for L2 CROWs as a function of cavity separation (black lines). Triangles indicate $Q(0)$, and circles indicate $Q(k_{Bz})$. All values are calculated using the TBA. We see from the figure that $Q(0)$ and $Q(k_{Bz})$ oscillate around the Q_o of the isolated cavity, shown by the dashed line. Interestingly, $Q(0)$ and $Q(k_{Bz})$ are always on opposite sides of Q_o. As a result, it is never the case that $Q(k)$ is larger or smaller than Q_o for all k. As the number of separation holes is increased, both $Q(0)$ and $Q(k_{Bz})$ approach Q_o. This trend is intuitive; in the limit of large separation, the CROW can be viewed as a chain of isolated cavities.

We next increase the length of the cavity. Results for L3 CROWs are shown by red lines in Fig. 5(a). It can be seen from the figure that $Q(0)$ and $Q(k_{Bz})$ again oscillate around the isolated cavity value. Moreover, the increase in the isolated cavity Q_o between L2 and L3 corresponds to an increase in $Q(k)$. Similarly, we can form CROWs from L4 or L5 cavities (blue and magenta lines in Fig. 5(a)). Within the family of L2 to L5 cavities, the CROW quality factor increases with the quality factor of the isolated cavity. This result corresponds to the intuitive argument presented above in (Section 2). As the quality factor of the isolated cavity increases, the components of its power spectrum inside the light line decrease. This also tends to decrease the leaky components of CROW power spectrum, which may be obtained from the cavity power spectrum via Fourier component sampling.

For each cavity length (or data color) shown in Fig. 5(a), we notice that there are nodes where $Q(0)$ and $Q(k_{Bz})$ cross. At these points, we expect $Q(k)$ to be flat. In Fig. 5(b), we plot $Q(k)$ for CROWs designed with a number of separation holes equal to the first node in Fig. 5(a). In all cases, the variation in $Q(k)$ is small compared to Fig. 5(a). For L3 and L4, the number of separation holes is equal to 3. We thus obtain designs for CROWs whose loss is similar to the isolated cavity across the entire band. For L2 and L5, the ideal separation is

#179666 - $15.00 USD Received 12 Nov 2012; revised 21 Dec 2012; accepted 10 Jan 2013; published 25 Jan 2013

non-integer. While loss values can be calculated within the TBA, it is not obvious how to achieve non-integer separations in a real CROW structure. However, we have verified via direct FDTD simulations that for the L2 cavity, simply using a CROW unit cell of 4.4*a* and allowing a slight overlap of circular holes at each edge of the cell yields a similarly flat $Q(k)$ trend to that pictured, though at somewhat higher values. We have also verified via FDTD simulations (not shown) that in L3, L4 and L5 cavities, the TBA method gives accurate results for $Q(k)$ provided that the number of separation holes is greater than 2.

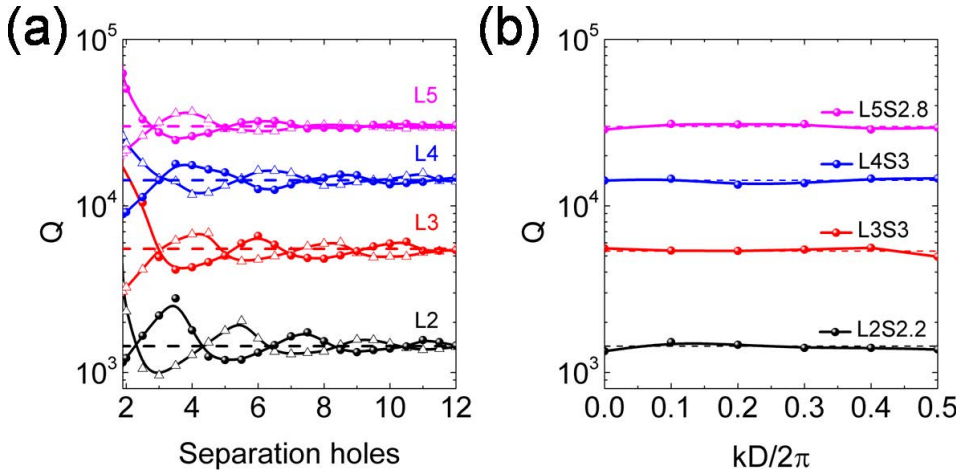

Fig. 5. (a) Quality factor for CROWs based on different constituent cavities. Triangles indicate $Q(0)$; circles indicate $Q(k_{BZ})$. Dashed lines show Q for single cavity. Calculations are performed using the TBA method. (b) $Q(k)$ for CROWs designed with a number of separation holes equal to the first node in (a).

5. Conclusions

In conclusion, we have applied the tight-binding approximation (TBA) to predict the radiation loss of CROW waveguides in photonic crystal slabs. Our formulation shows that as the quality factor of the isolated cavity increases, the CROW quality factor tends to increase as well. This trend can be understood within the light-cone picture of radiation loss. For both isolated cavities and CROWs, the quality factor is related to the spatial power spectrum of the fields above the photonic crystal slab. As the magnitude of the components inside the light cone decrease, the quality factor increases. Within the TBA, the CROW power spectrum can be approximated by sampling the isolated cavity power spectrum in Fourier space. The loss of the CROW thus tends to follow that of the isolated cavity. We have verified the validity of the TBA by comparing predicted values of $Q(k)$ for L2 CROWs with those obtained by direct simulation.

Importantly, our method allows the calculation of the wave-vector dependent CROW quality factor for a range of cavity separations from a single simulation of the isolated cavity fields. As a result, it is possible to scan various CROW configurations with minimal computational power. In particular, we demonstrate that it is possible to design waveguides with low, flat losses across the entire Brillouin zone, even at small intercavity separations.

We expect our results to be useful for a range of applications. For slow- and stopped-light applications, the fidelity of signal transmission at the end of a delay line depends on achieving low, flat loss across the signal bandwidth. In coupled-cavity lasers, the ability to tailor the $Q(k)$ loss profile could provide a useful method to control the effects of mode competition and tune the directional output of the laser. Lastly, in the context of light-assisted self-assembly above photonic-crystal slabs [28,29], our method may facilitate the design of large-area, coupled-cavity modes with high quality factor that nevertheless couple to normally-incident radiation.

#179666 - $15.00 USD Received 12 Nov 2012; revised 21 Dec 2012; accepted 10 Jan 2013; published 25 Jan 2013

Acknowledgments

The authors thank Ningfeng Huang for his help with dispersion relation simulations. This work was funded by the Army Research Office under Award No. 56801-MS-PCS. Computing resources were provided by the USC HPCC.

#179666 - $15.00 USD Received 12 Nov 2012; revised 21 Dec 2012; accepted 10 Jan 2013; published 25 Jan 2013